Echinoderm-inspired Tube Feet for Robust Robot Locomotion and Adhesion

Michael A. Bell[1,2], Isabella Pestovski[1,2], William Scott[3], Kitty Kumar[4], Mohammad K. Jawed[4], Derek A. Paley[3], Carmel Majidi[4], James C. Weaver[2], Robert J. Wood[1,2]

***Abstract*— Movement in echinoderms is facilitated by the coordinated activity of thousands of individually addressable and reversibly adhesive tube feet. To investigate the potential applicability of these unique biological actuators as a locomotory structure for robotics applications, we describe here the design, fabrication, and evaluation of an elastomeric structural analogue. The synthetic tube feet were modeled similar to that of a bi-stable deformable dome, containing an embedded magnet to facilitate the reversible attachment to ferromagnetic materials. Two unique robots have been developed using the bi-stability of these domes – CircleBot, which is capable of moving on ferrous surfaces using a pull and roll technique, and PlanarBot, which uses a programmed deflection direction in the domes to move in a plane.**

I. Introduction

Echinoderms are a remarkably agile group of marine invertebrates [1] and in recent years have provided a great deal of inspiration for the design and fabrication of a wide range of soft robotic actuators [2], [3], [4], [5]. While most of these prior studies have focused on replicating their penta-radial body plans or, in the case of sea stars, their large-scale arm movements [6], [7], we instead have directed our present efforts toward developing a series of tube foot-inspired actuators, which complements other reversible adhesion mechanisms developed in recent years [8], [9], [10], [11], [12], [13]. In sea stars, the tube feet are highly maneuverable hydraulically actuated cylindrical projections located on the animal's oral surface, each of which is terminated by a reversibly adhesive disk-like structure (Figure 1) [14]. The coordinated action of thousands of these individual tube feet results in the large scale movement of these species across a wide range of heterogeneous topographies. Inspired by their highly distributed functionality and robust reversible adhesion, we developed a synthetic tube foot structural analogue for incorporation into a wide range of robots, two of which are highlighted here.

In the tube feet of most echinoderm species (sea stars, sea cucumbers, and sea urchins), reversible attachment is accomplished via a duo-gland adhesion system [15], which is based on the controlled sequential secretion and degradation of protein-based underwater glues. In a robotic analogue however, the implementation of this strategy is not tractable using conventional fabrication approaches employed in the field of soft robotics. To mitigate these fabrication challenges, we instead chose to focus on a more novel, robust and scalable alternative that incorporates small permanent neodymium magnets for the reversible adhesion to ferromagnetic surfaces. In addition, we've incorporated a unique bi-stable deformable dome structure with an asymmetrical rib feature into our tube foot analogue that facilitate a robot's movement in a preprogrammed direction.

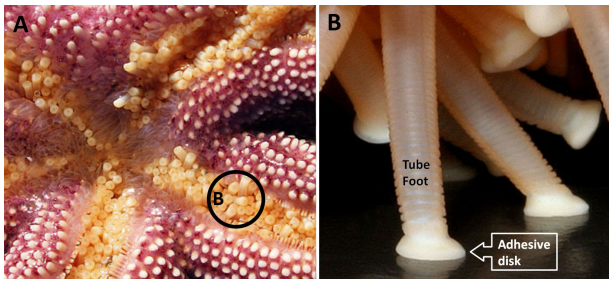

Fig. 1. (A) Located on the oral surface of a sea star along the arms are thousands of individually actuatable tube feet, (B) each of which is terminated by an adhesive disk.

II. Tube Foot Design, Fabrication and Testing

The tube foot structural analogs exhibit a bi-stable dome-like geometry, with the default molded shape in the retracted state [16], [17]. Iterations of geometries are numerically studied using finite element analysis and experimentally validated as described below.

A. Tube Foot Design and Fabrication

The 3D geometry of the tube foot is based on a fully parameterized 2D sketch that is revolved to produce a solid body. In the case of the programmed deflection direction (as discussed in Sec. II-C), a loft extruded rib is created on both the positive and negative mirrored sides of the dome membrane to create an asymmetry that biases the buckling trajectory to create a preferential direction of motion. Figure 2 shows the cross-section of an exemplary tube foot. The base mating geometry of the foot remained universal such that the same characterization rigs could be employed – and various robots (including the CircleBot and PlanarBot described here) could share feet. Parameters related to the

[1]John A. Paulson School of Engineering and Applied Sciences, Harvard University, 60 Oxford Street, Cambridge, MA 02138

[2]Wyss Institute for Biologically Inspired Engineering, Harvard University, 3 Blackfan Circle, Boston, MA 02115

[3]Department of Aerospace Engineering and Institute for Systems Research, University of Maryland, 3150 Glenn L. Martin Hall, College Park, MD 20742

[4]Department of Mechanical Engineering, Carnegie Mellon University, 5000 Forbes Avenue, Pittsburgh, PA 15213

dome angle, thickness, and actuation length are routinely modified in order to maintain a bi-stable architecture while simultaneously maximizing magnet retention throughout development.

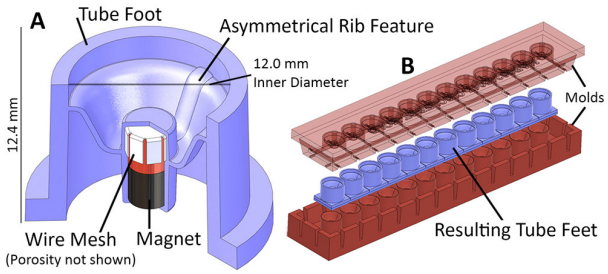

Fig. 2. (A) Schematic isometric cutaway overview of a single tube foot and (B) the molds for the fabrication of a linear tube foot array.

The tube foot molds (and the robot bodies with their associated fluid distribution networks) are 3D printed using an Objet Connex 500 3D printer (Stratasys, Eden Prairie, MN, USA) from VeroClear (RGD810) material. For the PlanarBot, the tube feet are produced in a nine-cavity mold with appropriate gates and runners for material evacuation during the molding process. The CircleBot utilizes a 1×12 tube foot array that can be easily stretched and secured over the CircleBot frame. Figure 2B shows the top and bottom molds with the resulting tube foot array in between.

B. Molding Process and Magnet Encapsulation

Each tube foot contains a single encapsulated magnet within the dome tip to facilitate adhesion to ferrous substrates. Stabilizing the magnet within the center of the volume during elastomer encapsulation while preventing the magnet from pulling out of the silicone material during actuation and adhesion presents a challenge [18]. To address both issues, thin metal wire meshes (RadioScreen^{TM}, Less EMF Inc., Latham, NY, USA) are laser cut in a star-like geometry and surround each magnet during the molding process. The wire mesh allows the silicone to flow around the magnet and subsequently acts as a barrier to prevent the magnet from ripping through the surrounding elastomer. To align the magnet within the encapsulation volume, additional magnets are placed within the exterior of the mold such that the encapsulated magnet maintains a stable geometry during the molding process.

The silicone molding material is Smooth-On (Macungie, PA, USA), Smooth-Sil 950 for the PlanarBot and Smooth-Sil 945 for the CircleBot, and 4% by weight Smooth-On Plat-Cat accelerator is added to the pre-polymer to accelerate the curing process. During molding, Ease Release 200 (Mann Formulated Products, Macungie, PA, USA) is used as a release agent for all surfaces of the mold. A small amount of Smooth-Sil is first poured into the top mold, degassed, and then the metal wire mesh is pushed through into the appropriate cavities, which allows complete infiltration of the elastomer. Magnets are inserted shortly after, followed by the remaining Smooth-Sil. The molds are then married, clamped and placed in a pressure chamber until fully cured.

C. Modeling, Behavior and Mechanics

In the early stages of the tube foot design process, continuous feedback is provided by finite element simulations (Abaqus Standard 6.12; SIMULIA, Providence, RI, USA) in order to understand the factors controlling dome deformation and the directional control of the resulting buckling behavior (Figure 3 and described below). In order to capture the large deformations involved in the bistable structure under pressurization, the elastomer is treated as a Neo-Hookean solid with shear modulus 1.875 MPa and elastic coefficients of $C_1 = 0.938$ MPa and $D_{10} = 5.33 \cdot 10^{-2}$ MPa^{-1} (values derived from the Smooth-Sil technical data sheet). These values correspond to compressible hyperelasticity, with a bulk to shear modulus ratio of 20. The surface mesh of the tube foot with and without ribs is constructed using second order tetrahedral hybrid elements, Abaqus code C3D10 and C3D10H, respectively, and the pneumatic actuation of the tube foot is simulated by applying pressure equivalent to 48 kPa to the top surface in the y-direction (Figure 3B). Gravity and self-contact during deformation are ignored in the simulations. The initial configuration of the model tube foot in the FEA is the same as in the experimental tests, with the foot clamped along the base flange.

The simulated behavior of the tube foot upon pressurization is presented in Figure 3. In the case of the tube foot structure with the smooth dome surface (Figure 3A), the elastic membrane buckles asymmetrically, which results in probabilistic deflection of the magnet in the direction determined by structural and material imperfections. Upon further pressurization, the quasi-stable structure deforms and stabilizes into the symmetrical second stable state. With the objective to minimize the detachment force, we optimize the dome geometry for maximum rotation angle of the magnet with respect to the vertical y-axis. In particular, we study the interrelationship between the slant angle θ (Figure 3B) of the dome wall and maximum rotation angle of the magnet in a quasi-stable state. As presented in Figure 3C, the magnet deflects farther away from the y-axis with the decrease in the slant angle from $\theta = 75^\circ$ to 0°. The domes with slant angle greater than 75° do not show a secondary stable state upon retraction. To avoid possible failure at sharp edges created during casting and molding process, we select an optimized dome geometry with the dome slant angle of 15°.

With the addition of the asymmetrical axial rib feature (Figure 3D-F), the asymmetry in the deformation are directly influenced by the rib location. This programmed asymmetry in the deformation regulates the deflection direction of the magnet, which we verify both numerically (Figure 3D), and experimentally (Figure 3F). Since the critical load required for the induction of this buckling behavior is lower than that which is observed in the smooth-domed control, the location of the axial rib feature can be tuned in order to achieve a specific directional deformation (a design element that is required for the successful operation of the PlanarBot).

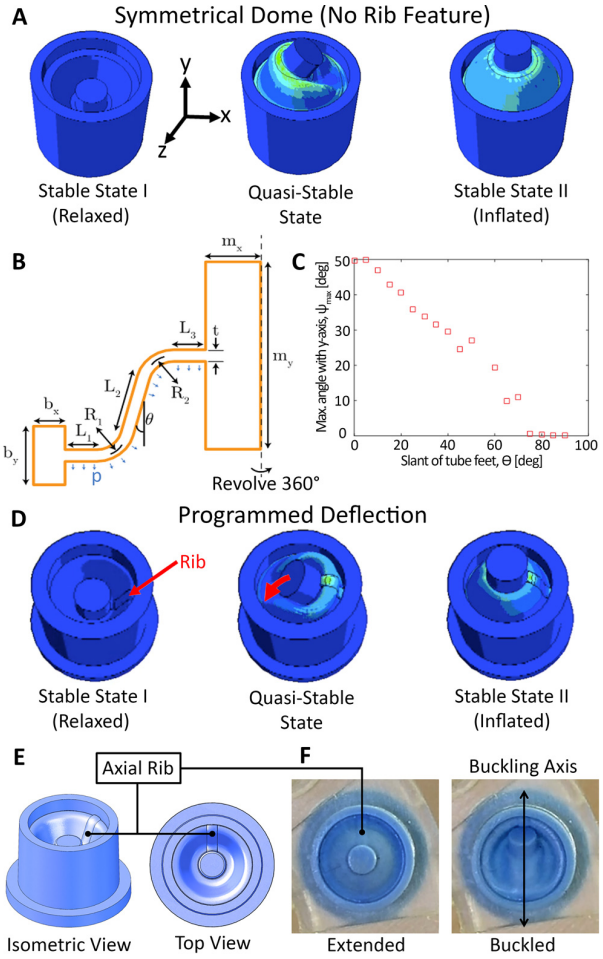

Fig. 3. (A) Simulated buckling behavior of tube foot without the asymmetrical axis rib feature. (B) Geometry of the tube foot with the dome-shape elastomer membrane (L_1 = 1 mm, L_2 = 2 mm, L_3 = 1 mm, R_1 = 1mm, R_2 = 1mm, t (membrane thickness) = 0.4 mm, m_x = 1.7 mm, m_x = 6.4 mm, b_x = 1 mm (irrelevant), b_x = 2 mm (irrelevant) and slant angle θ. (C) Rotation angle (ψ) of the magnet with respect to the vertical y-axis as a function of slant angle (θ) of the dome wall. Simulated (D) and experimental (F) buckling behavior of tube foot designed with the asymmetrical axial rib feature (E). The addition of rib element results in controlled directional deflection of the embedded magnet.

D. Experimental Characterization

Each tube foot used in the CircleBot contains an N52 grade cylindrical magnet, 1/8" dia. x 1/4" long (D24-N52, K&J Magnetics, Plumsteadville, PA, USA). The pull force of each magnet is 4.67 N (as reported by the manufacturer) when directly in contact with a ferrous surface. Through tensile testing measurements performed on an Instron 5566 (Instron, Norwood, MA, USA), however, the pull-off force of the encapsulated magnet behind the metal mesh and silicone stack-up is 3.51 N as seen in Figure 4. A second test is then performed with the Instron stationary and vacuum applied to the tube foot as tensile force is measured. During retraction, the dome of the tube foot buckles, which causes the magnet to rotate and eventually release with a maximum tensile force of only 1.10 N. Compared to the nominal strength of the magnet, dome buckling results in a two thirds reduction in the detachment force, demonstrating that the buckling instability and the bistable mechanics of the tube foot allows for controlled detachment with significantly less energy.

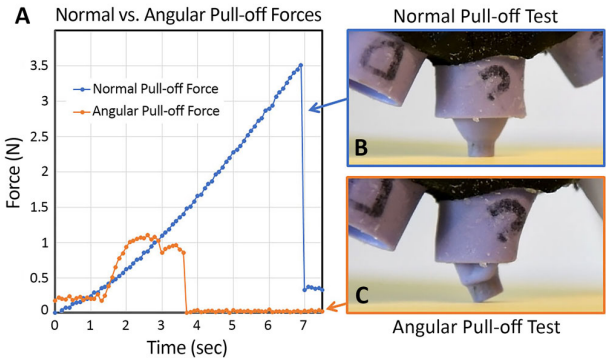

Fig. 4. (A) Normal vs. angular pull-off forces of the embedded magnet detaching from a ferrous surface. (B) Demonstration of normal tensile pull-off test, and (C) demonstration the rotation due to dome buckling, which produces significantly less force upon retraction.

III. CircleBot Demonstrator

The CircleBot (Figure 5) demonstrates the concept of integrated robust adhesion, ease of release and rotates by actuating or retracting one of the four sets of tube feet (denoted by groups A, B, C, and D). In order to optimize the CircleBot's gait for a coordinated forward motion, a mathematical motion model is developed and simulations are carried out to identify the specific order of tube foot actuation to achieve a rolling motion, the results of which are verified experimentally as described below. Though the model is idealized, with damped springs taking the place of the soft tube feet, we demonstrate that numerical simulations match closely with the motion of the experimental device.

A. Mathematical Gait Model

We model the CircleBot as a rigid body moving in a plane with mass m and moment of inertia I as follows: The shape of the body is a regular polygon with $n = 12$ sides, and apothem distance a, so that each side has length $l_s = 2a\tan(\pi/n)$. The radial angle between sides is $\alpha = 2\pi/n$. A pneumatic tube foot actuator is attached at the midpoint of each side, having a base with width w and length l_0 out from which the magnetic tip can extend, with a pressure-controlled nominal distance $l_i(u_i)$, where u_i is a control input representing the applied pressure for foot $i = 1, \ldots, n$.

If we let $\mathbf{r} = (x, y)^T \in \mathbb{R}^2$ be the location of the center of the robot in an inertial coordinate frame, and $\theta \in \mathbb{S}$ its orientation relative to that frame, then the nominal, or unforced, location of the tip of tube foot i is

$$\mathbf{r}_i = \begin{pmatrix} x \\ y \end{pmatrix} + R(\theta + \alpha i) \begin{pmatrix} a + l_0 + l_i(u_i) \\ 0 \end{pmatrix}, \qquad (1)$$

where R is the standard 2D rotation matrix.

If the x-axis represents a solid ferromagnetic surface, such that no part of the robot can pass through it, locomotion can

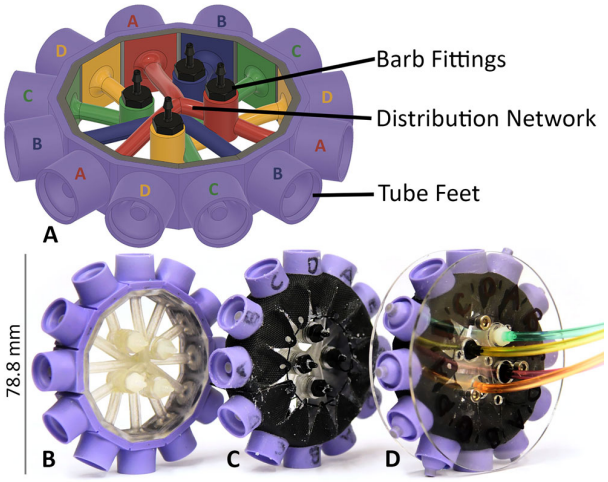

Fig. 5. (A) CAD model of CircleBot which includes four (color-coded) barbed input fittings, and a circular array of tube feet. (B-D) Fabrication steps of the CircleBot. (B) A silicone molded linear tube foot array is stretched around a frame. (C) A laser cut nylon sleeve is then placed around the tube feet and thread is used to compress the sleeve to ensure a good seal between the feet and the internal barb fittings. (D) Two 1.5 mm disk wheels are placed on either side of the CircleBot for balance and tubing is installed.

be achieved through controlled interaction between the tube feet and the surface.

The equations of motion for the rigid body are

$$\begin{aligned} m\ddot{x} &= mg\cos\gamma + \sum F_i^x \\ m\ddot{y} &= mg\sin\gamma + \sum F_i^y \\ I\ddot{\theta} &= \sum \tau_i, \end{aligned} \tag{2}$$

where F_i^x, F_i^y, and τ_i are the forces and torque exerted on the robot due to tube foot i, and g is the gravitational acceleration acting in direction γ.

1) Tube foot attachment: In a simplified model for the magnetic interaction between the tube foot and the surface, each tube foot has a binary state of attachment or detachment. When a tube foot is not attached to the surface, no external forces act on it. In contrast, the tube foot becomes attached when its distance to the surface is less than or equal to a threshold attachment distance y_a and the location of the tube foot tip becomes fixed, at $\mathbf{p}_i = (x_i, 0)^T$. When the tube foot is attached, it can exert both normal and shear forces on the surface, which depend on the material properties of the both the magnet and the surface. In the normal direction, F_d is the force of detachment (shown in Figure 4B), and once the force exerted by the tube foot in the direction normal to the surface exceeds F_d, the tube foot detaches.

2) Tube foot deformation: The relationship between deformation and applied force on the tube foot is modeled as a damped spring with spring constant k and damping constant d. The applied force thus varies linearly with the displacement of the actual tube foot tip location $\mathbf{p}_i$ from its nominal location $\mathbf{r}_i$, with $\mathbf{F}_i = (F_i^x, F_i^y)^T = k(u_i)(\mathbf{p}_i - \mathbf{r}_i) - d\,\dot{\mathbf{r}}_i$. The applied torque τ_i about the center of the CircleBot due to $\mathbf{F}_i$ is the scalar part of the vector $(\mathbf{p}_i - \mathbf{r}) \times \mathbf{F}_i$.

The linear damped spring model was chosen for the tube foot for its simplicity and low number of parameters while still retaining the qualitative behavior of the CircleBot device. To achieve higher fidelity, more features may be added to the model, such as allowing the spring constant to vary with the applied pressure in the tube foot, or specifying a nonlinear relationship between force and displacement.

B. Control design

The goal is to design a gait, or periodic trajectory in the applied control variables, that gives rise to a repeated net displacement of the robot in a desired direction. For design of a rolling trajectory, we separate the action of a single tube foot into four distinct phases:

1) Reaching out: the free tube foot extends outward, reaching towards the surface;
2) Pulling in: once attached, the tube foot retracts in order to pull the robot in that direction;
3) Pushing out: as the robot rolls over the tube foot (still attached but fully retracted) it begins to extend again, to push the robot along; and
4) Detachment: at full extension, the tube foot pulls in sharply to achieve detachment until the robot rolls around far enough to start the cycle again.

The possible number of tube feet attached at any given time will depend on the geometry of the robot. The number of feet n determines the angle $\alpha = 2\pi/n$ between the feet. The maximum extended length determines at what orientation the tube foot can become attached. If l_e is the maximum extended length under high pressure input, then the maximum angle from vertical where attachment can occur, for the robot up against the surface with $y = a + l_0$, is $\bar{\theta} = \cos^{-1}((a + l_0)/(a + l_0 + l_e))$. Climbing ability on an inclined surface will depend on the possible number of attached feet, since if the robot cannot stay attached to the surface in a static configuration it will not be able to climb it either.

Closed-loop feedback control can be achieved if the robot has an onboard sensor to measure its orientation, such as an accelerometer. Let u_i be the control input to foot i, taking values in the set $\{-1, 0, 1\}$ corresponding to applied vacuum, vent, and applied pressure, respectively. We propose a control law based on the four phases of foot motion described above:

$$u_i(\theta_i) = \begin{cases} +1, & \theta_{pull} < \theta_i \leq \theta_{reach} \\ 0, & \theta_{push} < \theta_i \leq \theta_{pull} \\ +1, & \theta_{detach} < \theta_i \leq \theta_{push} \\ -1, & \theta_{end} < \theta_i \leq \theta_{detach}, \end{cases} \tag{3}$$

where $\theta_i = \theta + i\alpha$ is the orientation of foot i. Parameters $\theta_{reach} > \theta_{pull} > \theta_{push} > \theta_{detach} > \theta_{end}$ refer to switching surfaces, such that the control input changes as the foot orientation crosses those values. By choosing $\theta_{reach} - \theta_{end} = 2\pi/3$, we ensure that only one foot out of a given control group is under control at a given moment—as one foot, i, reaches θ_{end}, the next foot controlled by the same input, $i + 4$, reaches θ_{reach}, assuming $\dot{\theta} < 0$ (clockwise rolling).

C. Simulation

A simulation is performed in MATLAB version R2017a (Mathworks, Inc, Natick, MA, USA) based on forward Euler integration with a fixed time step $\Delta t = 0.001$ s. The following parameter values are derived from the fabricated device: $n = 12$, $a = 39.4$ mm, $w = 13.9$ mm, $l_0 = 10.4$ mm, $l_e = 4.5$ mm, $m = 35.3$ g, $I \approx ma^2 = 5,480$ g-mm^2 (assuming most mass is concentrated at radius a), $y_a = 1$ mm, $F_d = 3.51$ N (based on normal pull-off test), $g = 9.81$ m/s^2, and $\gamma = -\pi/2$ (gravity directly downwards). The extended length of tube foot varies with the applied pressure. For vacuum, $l_i = -l_e$; for ambient pressure, $l_i = 0$; and for high pressure, $l_i = l_e$. The spring constant of $k = 0.743$ N/mm is estimated from the slope of the Force-displacement curve from the normal pull-off test. The tube foot springs are assumed to be highly damped with a damping ratio $\zeta = 0.7$, corresponding to $d = 2.86$ N-s based on the spring constant and the mass of an individual tube foot measured as 1.38 g.

Figure 6 shows snapshots before, during, and after a single step in a rolling trajectory for the experimental device along with a simulation using the same input timing.

D. Experimental Results

The fabricated CircleBot is tested using a custom LabVIEW 2016 (National Instruments, Austin, TX, USA) GUI sequencer and two 3-way valves per channel, with four channels in total, which enables each tube foot to have positive, negative, and ambient air pressure. As no more than four tube feet can be in contact through any sequence, only four channels are required to drive a total of 12 tube feet (three feet per channel), which greatly reduces the required number of tubes and control lines. In addition, electro-pneumatic regulators are employed to adjust the positive and negative pressures for each test. Each channel is supplied with identical positive and negative pressures, which are maintained during continuous cycling once the required actuation and retraction pressures are determined.

Figure 6 shows 1/4 of a cycle, switching the normal tube foot on the substrate from "B" to "C". Step 2 shows the transition step where all tube feet can be observed momentarily being actuated as a rotation is occurring.

The CircleBot achieves a velocity of 3.2 mm/sec with minimally tunned actuation timing (with a 78.8 mm diameter CircleBot, this is 0.04 body lengths per second (BL/s)). While the current CircleBot design is not able to climb inclines greater than ca. 15°, which is likely due to the lack of movement during the step transition and weight of the robot, the presence of additional parallel tube foot arrays or the incorporation of larger, stronger magnets will likely provide enough additional adhesive force to allow the robot to climb walls.

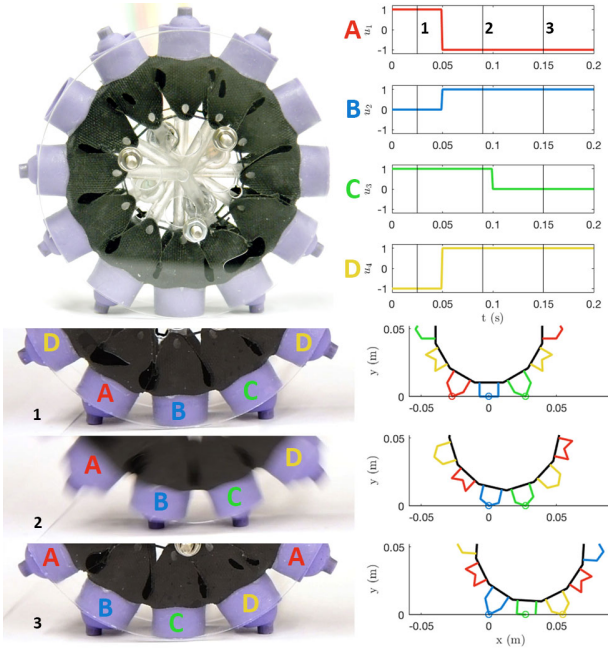

Fig. 6. Top left: CircleBot attached to a level flat ferrous surface. Bottom left: Steps 1-3 as shown on video capture for a 1/4 cycle. Right: Simulation of CircleBot under the open-loop control. Top right: Input trajectories vs. time for the four inputs, with colors matching the controlled tube feet on the snapshots. Input values of -1, 0, and 1 correspond to vacuum, ambient, and high pressure inputs, respectively. In both the modeled motion (bottom right) and the corresponding input trajectories (top right), the colors are matched to the manifold architecture diagrammed in Figure 5. Bottom Right: Snapshots of the system state at the start of each step cycle.

IV. PlanarBot Demonstrator

Guided by the FEA simulations investigating induced directionality during tube foot buckling, a PlanarBot is fabricated to exploit this directional anisotropy. The PlanarBot design consists of up to 12 tube feet hydraulically controlled through the use of a syringe pump, and through multiple cycles, can move along a path described by the rib orientation. Figure 7 captures the actuation "kick" of the PlanarBot from rest to standing, and retracting. Each foot contributes to the locomotion of the robot on both actuation and retraction cycles.

The PlanarBot, as seen in Figure 7, is constructed with a central 3D printed hub that allows for rapid iteration on tube foot design. The tube feet fit over a barbed feature, and a 3D printed snap clip retains each of the tube feet (while allowing rapid replacement and repositioning for the exploration of different gait configurations). The hub also contains four threaded inlet ports for barbed fittings and, through its four internal chambers, equally distributes a channel's pressure to the three attached hydraulic distribution tubes. For this demonstrator, two channels are merged to control six tube feet at once.

The tube feet achieve a linear motion of 4.4 mm per cycle using hydraulic actuation, with a full cycle taking 3.87 seconds or 1.14 mm/sec. As the PlanarBot body size is arbitrary, if we only consider a single tube foot actuator, this equates to 0.078 BL/s, due to limitations of the syringe

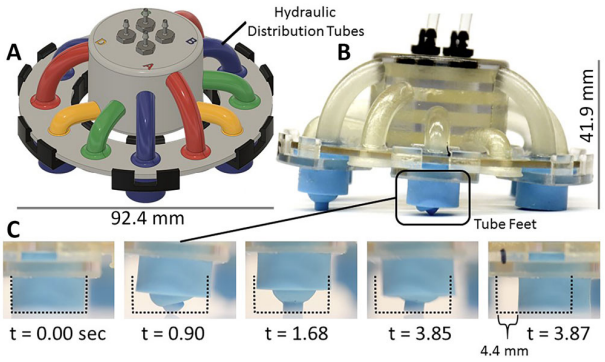

Fig. 7. PlanarBot design with up to four channels, and a fabricated PlanarBot produced through 3D printing (A-B). Results of the tube foot gait cycle with a total movement per cycle of 4.4 mm (C).

pump speed in the test rig (which is on par or exceeds tube foot actuation speeds reported previously for living sea stars, when normalized for tube foot length [1], [19]).

Hydraulics are required in place of a pneumatic system since the expansion of air in a tube foot post-bucking is uncontrollable, which results in very quick impulses from the foot (5 ms). These impulses can not be adequately dampened with magnetic forces, weights, or surface friction in order to achieve controlled linear motion. In contrast, hydraulic fluid is incompressible and the tube foot expansion is limited by the compression rate of the syringe pump, resulting in an amplified kicking motion and locomotion with a controlled linear response—features that are not possible with pneumatics. If pneumatic actuation is employed, however, we could potentially achieve a seven fold increase in speed (0.55 body lengths per second).

V. Conclusions and Future Directions

In the present study, a mechanical analog of an echinoderm's tube foot was explored and demonstrated for robust adhesion and locomotion. The tube foot fabrication strategy employed traditional techniques from soft robotics, with new methods introduced to embed magnets during the molding process. FEA simulations demonstrated a buckling instability that occurred during tube foot actuation that could be harnessed for controlling directionality via the incorporation of an asymmetric axial rib-like feature. Using these design strategies, the CircleBot implementation illustrated robust attachment of the magnetic tube feet and ease of release, while tube feet with programmed directional deformation were demonstrated through the PlanarBot to create a kick-like gait.

To achieve additional functionality, future iterations of the the CircleBot demonstrator could incorporate parallel arrays of tube feet allowing vertical surface climbing. It could also gain the ability to steer by incorporating additional parallel tube feet arrays with a slight angular offset, and through differential controlling of the actuation timing. Lastly, the CircleBot could turn into a full SphereBot and take the form of a controlled-movement tumbleweed.

Future modifications to the PlanarBot model would include more complex programmable deformation directions of a larger tube foot array, which would facilitate omnidirectional locomotion. By combining programmed tube foot buckling direction with magnetic attachment and release, the Planarbot would be able to navigate any ferrous object. With a modified hub geometry into which the tube feet integrate, such as a bellow-type actuator [20], it could feasibly traverse substrates with nonuniform topographies such as the hull of a ship.

Small fluidic actuators are highly advantageous in soft robotic systems as distributed actuator arrays can conform around surfaces to provide uniform attachment forces. The soft robot would also be highly robust, allowing many actuators to be potentially impaired without compromising the locomotion or grasping performance (compared with motion or manipulation using a small number of actuators). On a large-scale – mimicking the number of tube feet in a large sea star – one could foreseeably see adhesion forces in the range of hundreds to thousands of kilograms of pull force [1]. When a large load is applied normal to the plane of attachment in a living sea star, the adhesion is frequently stronger than the cohesive strength of the soft tissue, and the tube feet will fail internally. From an engineering perspective in a robotic analogue, this effect would be highly undesirable (as there is no internal healing modes), but this information would enable more cost-effective fabrication by balancing the known strength of the elastomer with that of the pull force of the encapsulated magnets.

A future direction to take the tube foot concepts and the demonstrators is in a fully untethered, teleoperated, or autonomous robot. The pressures required to actuate both types of tube feet described here are on-par with or significantly below those pressures employed for the actuation of previous soft robotic prototypes designed for deep sea exploration [20]. In addition, the opportunity to create fully autonomous robots can be achieved (depending on the desired habitat of interest) through the incorporation of small pneumatic, hydraulic, or peristaltic pumps as has been demonstrated on previous untethered soft robotic systems [2]. Other advantages of the locomotory scheme described here is that it results in very low deflection of the robot along the z-axis, while possessing the ability to maintain high adhesion strength during all stages of forward motion. As such, these soft robotic prototypes (especially the PlanerBot configuration) could subsequently maintain a low profile body plan for maneuverability in high flow situations and could therefore be useful in applications including deep sea salvaging and exploration, inspection of pipes and structures, or the inspection of ship hulls.

Acknowledgments

The authors gratefully acknowledge support from the Office of Naval Research (award # N00014-17-1-2063) and the Wyss Institute for Biologically Inspired Engineering. We thank Larry Friesen for permission to use the tube foot image in Figure 1.

REFERENCES

[1] R. H. Morris, D. P. Abbott, and E. C. Haderlie, *Intertidal Invertebrates of California*. Stanford: Stanford University Press, 1 ed., 1980.

[2] R. F. Shepherd, F. Ilievski, W. Choi, S. A. Morin, A. A. Stokes, A. D. Mazzeo, X. Chen, M. Wang, and G. M. Whitesides, "Multigait soft robot," *Proceedings of the National Academy of Sciences*, vol. 108, no. 51, pp. 20400–20403, 2011.

[3] A. Sadeghi, L. Beccai, and B. Mazzolai, "Design and development of innovative adhesive suckers inspired by the tube feet of sea urchins," in *Proceedings of the IEEE RAS and EMBS International Conference on Biomedical Robotics and Biomechatronics*, (Rome, Italy), pp. 617–622, IEEE, 2012.

[4] S. Mao, E. Dong, S. Zhang, M. Xu, and J. Yang, "A new soft bionic starfish robot with multi-gaits," in *2013 IEEE/ASME International Conference on Advanced Intelligent Mechatronics: Mechatronics for Human Wellbeing, AIM 2013*, (Wollongong, NSW), pp. 1312–1317, IEEE, 2013.

[5] T. Umedachi, V. Vikas, and B. A. Trimmer, "Highly deformable 3-D printed soft robot generating inching and crawling locomotions with variable friction legs," in *IEEE International Conference on Intelligent Robots and Systems*, (Tokyo), pp. 4590–4595, IROS, 2013.

[6] S. Mao, E. Dong, M. Xu, H. Jin, F. Li, and J. Yang, "Design and development of starfish-like robot: Soft bionic platform with multi-motion using SMA actuators," in *2013 IEEE International Conference on Robotics and Biomimetics, ROBIO 2013*, (Shenzhen), pp. 91–96, IEEE, 2013.

[7] W. L. Scott and D. A. Paley, "Geometric gait design for a starfish-inspired robot with curvature-controlled soft actuators," in *Proc. ASME Dynamic Systems and Control Conference*, (Tysons, VA), p. V002T07A005, ASME, 2017.

[8] E. Arzt, S. Gorb, and R. Spolenak, "From micro to nano contacts in biological attachment devices," *Proceedings of the National Academy of Sciences*, vol. 100, no. 19, pp. 10603–10606, 2003.

[9] B. K. Ahn, S. Das, R. Linstadt, Y. Kaufman, N. R. Martinez-Rodriguez, R. Mirshafian, E. Kesselman, Y. Talmon, B. H. Lipshutz, J. N. Israelachvili, and J. H. Waite, "High-performance mussel-inspired adhesives of reduced complexity," *Nature Communications*, vol. 6, p. 8663, 2015.

[10] C. Zhong, T. Gurry, A. A. Cheng, J. Downey, Z. Deng, C. M. Stultz, and T. K. Lu, "Strong underwater adhesives made by self-assembling multi-protein nanofibres," *Nature Nanotechnology*, vol. 9, pp. 858–866, 2014.

[11] H. Lee, B. P. Lee, and P. B. Messersmith, "A reversible wet/dry adhesive inspired by mussels and geckos," *Nature*, vol. 448, pp. 338–341, 2007.

[12] D. Santos, B. Heyneman, S. Kim, N. Esparza, and M. R. Cutkosky, "Gecko-inspired climbing behaviors on vertical and overhanging surfaces," in *Proceedings - IEEE International Conference on Robotics and Automation*, (Pasadena, CA), pp. 1050–4729, IEEE, 2008.

[13] P. Glass, E. Cheung, and M. Sitti, "A legged anchoring mechanism for capsule endoscopes using micropatterned adhesives," *IEEE Transactions on Biomedical Engineering*, vol. 55, no. 12, pp. 2759 – 2767, 2008.

[14] R. Santos, "Adhesion of echinoderm tube feet to rough surfaces," *Journal of Experimental Biology*, vol. 208, pp. 2555–2567, 2005.

[15] E. Hennebert, R. Santos, and P. Flammang, "Echinoderms don't suck: evidence against the involvement of suction in tube foot attachment*," *Zoosymposia Echinoderm Research Zoosymposia*, vol. 7, no. 7, pp. 25–32, 2012.

[16] A. Brinkmeyer, M. Santer, A. Pirrera, and P. M. Weaver, "Pseudo-bistable self-actuated domes for morphing applications," *International Journal of Solids and Structures*, vol. 49, no. 9, pp. 1077–1087, 2012.

[17] A. Madhukar, D. Perlitz, M. Grigola, D. Gai, and K. Jimmy Hsia, "Bistable characteristics of thick-walled axisymmetric domes," *International Journal of Solids and Structures*, vol. 51, no. 14, pp. 2590–2597, 2014.

[18] S. W. Kwok, S. A. Morin, B. Mosadegh, J. H. So, R. F. Shepherd, R. V. Martinez, B. Smith, F. C. Simeone, A. A. Stokes, and G. M. Whitesides, "Magnetic assembly of soft robots with hard components," *Advanced Functional Materials*, vol. 24, no. 15, pp. 2180–2187, 2014.

[19] E. M. Montgomery, "Predicting crawling speed relative to mass in sea stars," *Journal of Experimental Marine Biology and Ecology*, vol. 458, pp. 27–33, 2014.

[20] K. C. Galloway, K. P. Becker, B. Phillips, J. Kirby, S. Licht, D. Tchernov, R. J. Wood, and D. F. Gruber, "Soft Robotic Grippers for Biological Sampling on Deep Reefs," *Soft Robotics*, vol. 3, no. 1, pp. 23–33, 2016.